

Topological invariants and phase diagrams for one-dimensional two-band non-Hermitian systems without chiral symmetry

Hui Jiang,^{1,2} Chao Yang,^{1,2} and Shu Chen^{1,2,3,*}

¹*Beijing National Laboratory for Condensed Matter Physics,
Institute of Physics, Chinese Academy of Sciences, Beijing 100190, China*

²*School of Physical Sciences, University of Chinese Academy of Sciences, Beijing 100049, China*

³*Collaborative Innovation Center of Quantum Matter, Beijing, China*

We study topological properties of one-dimensional non-Hermitian systems without chiral symmetry and give phase diagrams characterized by topological invariants ν_E and ν_{tot} , associated with complex energy vorticity and summation of Berry phases of complex bands, respectively. In the absence of chiral symmetry, we find that the phase diagram determined by ν_E is different from ν_{tot} . While the transition between phases with different ν_E is closely related to the band-touching point, the transition between different ν_{tot} is irrelevant to the band-touching condition. We give an interpretation for the discrepancy from the geometrical view by analyzing the relation of topological invariants with the winding numbers associated with exception points of the system. We then generalize the fidelity approach to study the phase transition in the non-Hermitian system and find that transition between phases with different ν_{tot} can be well characterized by an abrupt change of fidelity and fidelity susceptibility around the transition point.

I. INTRODUCTION

Topological phases of matter have been one of the most intriguing research subjects in condensed matter physics. Recently topological phases in non-Hermitian system have attracted great attention [1–37] partially motivated by the experimental progress on optical and optomechanical systems with gain and loss, which can be implemented in a controllable manner and effectively described by non-Hermitian systems [38–45]. Recent studies have unveiled that the topological properties of non-Hermitian systems may exhibit quite different behaviors from Hermitian systems, associated with some peculiar properties of the non-Hermitian Hamiltonian, e.g., biorthonormal eigenvectors, complex eigenvalues, the existence of exceptional points (EPs) and unusual bulk-edge correspondence [46–55]. Although non-Hermiticity brings some challenges for carrying out topological classification and properly defining topological invariants on biorthonormal eigenvectors [22, 23, 54], the non-Hermitian system with novel qualities has opened up new frontiers for exploring rich topological phenomena.

It is well known that symmetry and dimension play an important role in the study of topological properties [22–24, 56]. For one-dimensional (1D) topological systems with chiral symmetry, the topological properties of the Hermitian systems can be characterized by a winding number ν_s , which is closely related to the Berry phase across the Brillouin zone (Zak phase) of systems [16, 57, 58]. For the non-Hermitian system with chiral symmetry, one can generalize the definition of winding number ν_s as a topological invariant. Furthermore, due to the eigenvalue being complex, we need define another topological winding number ν_E , describing the vorticity of energy eigenvalues [11, 15]. The phase diagram of the non-Hermitian system with chiral symmetry can be well

characterized by ν_E and ν_s , which can take half integers. In a recent work [16], it was demonstrated that both ν_E and ν_s are related to two winding numbers ν_1 and ν_2 which represent the times of trajectory of Hermitian part of the momentum-dependent Hamiltonian encircling the EPs.

In this work, we study 1D non-Hermitian systems without chiral symmetry, which are found to exhibit quite different behaviors from their counterparts with chiral symmetry. In the absence of chiral symmetry, while ν_E remains to be a topological invariant, the Berry phase for each band is not quantized and the corresponding ν_s is no longer a topological invariant. Nevertheless, the summation of ν_s for all the bands, denoted by ν_{tot} , is still quantized and can be taken as topological invariant [6]. By studying a concrete two-band non-Hermitian model, we find that the phase diagram determined by the topological invariant ν_E is different from that characterized by ν_{tot} . While the phase boundaries of phase diagram characterized by ν_E correspond to the band-touching points of the non-chiral system, no band touching occurs at the phase boundaries of ν_{tot} . This is in sharp contrast to the chiral non-Hermitian system, for which the phase boundaries between phases with different ν_s also correspond to the band-touching points. To understand the discrepancy of phase diagrams of the non-chiral systems, we further unveil the geometrical meaning of the topological invariants ν_E and ν_{tot} . Similar to the chiral non-Hermitian system, we find that ν_E is related to the winding numbers ν_1 and ν_2 which count the times of trajectory of the Hermitian part of the Hamiltonian encircling the EPs of the non-chiral Hamiltonian. However, ν_{tot} is related to different winding numbers ν'_1 and ν'_2 associated with EPs of a Hamiltonian in the absence of the term breaking the chiral symmetry.

For the Hermitian system, besides the general Landau criteria for quantum phase transitions (QPTs), fidelity approach provides an alternative way to identify the QPT from the perspective of wave functions [59–63]. Generally one may expect that the fidelity of ground state shows an abrupt change in the vicinity of the phase transition point of the system as a consequence of the dramatic change of the structure of the ground state. So far the studies of fidelity as a measure of

* schen@iphy.ac.cn

QPTs are focused on Hermitian systems, for which either the Landau's energy criteria or the fidelity approach gives a consistent phase diagram. In this work, we shall generalize the fidelity approach to study phase transition in non-Hermitian systems. To our surprising, we find that both the fidelity and fidelity susceptibility exhibit obvious changes in the vicinity of phase boundaries of phases characterized by ν_{tot} , instead of ν_E . This suggests that the phase transition between phases with different ν_{tot} can be determined by the fidelity approach, whereas the transition between different ν_E is closely related to the band-touching (gap-closing) condition and can be determined by the generalized Landau's criteria.

The paper is organized as follows. In section II, we first give a general framework to expound the basic characteristics of two-band non-Hermitian system. In section III, we introduce a non-Hermitian model without chiral symmetry and analyze the spectrum of the system. We also calculate the topological invariant ν_E and give the phase diagram characterized by ν_E . In section IV, we calculate the other topological invariant ν_{tot} , associated with the Berry phase, and the phase diagram characterized by ν_{tot} . We find discrepancy of phase diagrams characterized by ν_E and ν_{tot} , and unveil that the two topological invariants are related to different winding numbers associated with the EPs of the Hamiltonian with and without chiral symmetry. We also analyse the effect of a hidden pseudo-inversion symmetry on the topological property of eigenstate. Then, we calculate the fidelity of a given eigenstate and the corresponding fidelity susceptibility to identify the phase transition characterized by ν_{tot} . A summary is given in the last section.

II. TOPOLOGICAL INVARIANTS OF 1D TWO-BAND NON-HERMITIAN SYSTEMS

In general, a two-band non-Hermitian system can be described by

$$\mathcal{H}(k) = \mathbf{h}(k) \cdot \boldsymbol{\sigma} = \mathbf{n}(k) \cdot \boldsymbol{\sigma} + i\boldsymbol{\gamma}(k) \cdot \boldsymbol{\sigma}, \quad (1)$$

where $\mathbf{h}(k)$, $\mathbf{n}(k)$ and $\boldsymbol{\gamma}(k)$ may include three components x, y, z and $\sigma_{x,y,z}$ is the Pauli matrix. In general, the non-Hermitian system can be divided into the summation of Hermitian and non-Hermitian part: $\mathbf{h}(k) = \mathbf{n}(k) + i\boldsymbol{\gamma}(k)$ with $\mathbf{n}(k)$ and $\boldsymbol{\gamma}(k)$ being real functions of k . The energy square of non-Hermitian Hamiltonian is: $E^2 = |\mathbf{n}|^2 - |\boldsymbol{\gamma}|^2 + 2i\mathbf{n} \cdot \boldsymbol{\gamma} := E_1^2 = E_2^2$ ($E_1 = -E_2$). It is clear that the two bands touch at zero when $\mathbf{n}(k) \perp \boldsymbol{\gamma}(k)$ and $|\mathbf{n}(k)| = |\boldsymbol{\gamma}(k)|$.

The eigenvalue $E_{1,2}$ is smoothly continuous with k . Since the eigenvalue is generally complex, we can represent it as $E_1 = |E|e^{i\theta_k} = -E_2$ with θ_k the angle of eigenvalue. As k goes across the Brillouin zone (BZ), we can always define the winding number of energy ν_E as [11, 15]

$$\nu_E = \frac{1}{2\pi} \oint dk \partial_k \text{Arg}(\Delta E) = \frac{1}{2\pi} \oint dk \partial_k \text{Arg}(E_1 - E_2). \quad (2)$$

For the Hermitian system, ν_E is always zero as θ_k takes either 0 or π . See appendix A for the detailed calculation of ν_E .

On the other hand, the eigenstates of non-Hermitian Hamiltonian (Eq.(1)) satisfy $\mathcal{H}(k)|\psi_{1,2}^R\rangle = E_{1,2}|\psi_{1,2}^R\rangle$, and $|\psi_{1,2}^R\rangle$ do not form an orthogonal basis. In order to describe non-Hermitian properties, we need also consider the eigenstates of \mathcal{H}^\dagger , $\mathcal{H}^\dagger(k)|\psi_{1,2}^L\rangle = E_{1,2}^*|\psi_{1,2}^L\rangle$, which together with $|\psi_{1,2}^R\rangle$ form biorthogonal vectors and fulfill $\langle\psi_i^L|\psi_j^R\rangle = \delta_{ij}$ by properly choosing the normalization $\langle\psi_{1,2}^L|\psi_{1,2}^R\rangle$. For simplicity, we choose

$$|\psi_{1,2}^R\rangle = \frac{1}{\sqrt{2E_{1,2}(E_{1,2} - h_z)}} \begin{pmatrix} h_x - ih_y & E_{1,2} - h_z \end{pmatrix}^T,$$

where the superscript T is transpose operation, and

$$\langle\psi_{1,2}^L| = \frac{1}{\sqrt{2E_{1,2}(E_{1,2} - h_z)}} \begin{pmatrix} h_x + ih_y & E_{1,2} - h_z \end{pmatrix}.$$

Similar to the definition of winding number related to the Berry phase of eigenstate in Hermitian system, one can generalize the definition ν_s directly to the non-Hermitian system [8, 16, 21], which can be written as

$$\nu_{s,\alpha} = \frac{1}{\pi} \oint dk \langle\psi_\alpha^L|i\partial_k|\psi_\alpha^R\rangle, \quad (3)$$

where $\alpha = 1, 2$ indicate the band labels. Substituting the concrete forms of $|\psi_\alpha^R\rangle$ and $\langle\psi_\alpha^L|$ into the above equation, after some simplifications, we can represent ν_s as (Appendix.B):

$$\nu_{s,\alpha} = \frac{1}{2\pi} \oint dk \frac{h_x \partial_k h_y - h_y \partial_k h_x}{E_\alpha(E_\alpha - h_z)}, \quad (4)$$

where E_1 and E_2 are eigenvalues of the non-Hermitian Hamiltonian.

For the case with chiral symmetry, it has been shown that both ν_E and $\nu_{s,\alpha}$ can only take some half-integers. In a recent work, it has been demonstrated ν_E and $\nu_{s,\alpha}$ are related to the winding numbers ν_1 and ν_2 of trajectory of the Hermitian part around two different EPs, respectively [16], and thus explain why they are topological invariant with half-integers. The phase diagrams can be determined by different values of either ν_E or $\nu_{s,\alpha}$, or equivalently ν_1 and ν_2 . For the general case without chiral symmetry, ν_E remains to be a topological invariant, however, $\nu_{s,\alpha}$ is generally a complex number which is not quantized, suggesting that $\nu_{s,\alpha}$ is no longer a topological invariant. Nevertheless,

$$\nu_{tot} = \nu_{s,1} + \nu_{s,2}$$

has been demonstrated to be a topological invariant, which takes integers [6]. As shall be discussed in detail in the following section, we find that phase boundaries of the phase diagram determined by ν_E is consistent with the band touching curves determined by $E_1 = E_2 = 0$. On the other side, we can also get a phase diagram determined by topological invariant ν_{tot} , which displays obviously different phase boundaries from phase boundaries determined by ν_E . To understand this discrepancy, we further analyze geometrical origins of ν_E and

ν_{tot} , associated to the Hamiltonian (7). While ν_E can be related to the winding numbers around to two EPs of the Hamiltonian (7) via $\nu_E = \pm \frac{1}{2}(\nu_2 - \nu_1)$, we find no relation of ν_{tot} with ν_1 and ν_2 , instead we have $\nu_{tot} = \nu'_1 + \nu'_2$, where ν'_1 and ν'_2 are winding numbers around EPs of the Hamiltonian in the absence of the chemical potential term.

III. MODEL AND SPECTRUM

For simplicity, we consider a 1D non-Hermitian model by choosing the Su-Schrieffer-Heeger (SSH) model as the Hermitian part of the non-Hermitian Hamiltonian, and introduce an off-diagonal non-Hermitian part by taking different hopping amplitudes along the right and left hopping directions in the unit cell [16, 54]. A diagonal non-Hermitian term is also introduced by alternatively adding imaginary chemical potential $\pm i\mu$ on the A/B-sublattice. Explicitly, the Hamiltonian is given by

$$H = \sum_n (t + \delta) c_{A,n}^\dagger c_{B,n} + (t - \delta) c_{B,n}^\dagger c_{A,n} + t' c_{A,n+1}^\dagger c_{B,n} + t' c_{B,n+1}^\dagger c_{A,n+1} + i\mu c_{A,n}^\dagger c_{A,n} - i\mu c_{B,n}^\dagger c_{B,n}, \quad (5)$$

with $t' = 1$ as the unit of energy in the following discussion. Under the periodic boundary condition, we can make a Fourier transformation: $c_{\alpha,n} = 1/\sqrt{N} \sum_k e^{ikn} c_{\alpha,k}$ where N is the number of the unit cells and α takes A or B. Then the Hamiltonian can be written in the form of

$$H(k) = \sum_k \phi_k^\dagger \mathcal{H}(k) \phi_k, \quad (6)$$

where $\phi_k^\dagger = (c_{A,k}^\dagger, c_{B,k}^\dagger)$, and

$$\mathcal{H}(k) = \begin{pmatrix} i\mu & t + \delta + e^{-ik} \\ t - \delta + e^{ik} & -i\mu \end{pmatrix} = \mathbf{n}(k) \cdot \boldsymbol{\sigma} + i\delta\sigma_y + i\mu\sigma_z. \quad (7)$$

Here the Hermitian part is $\mathbf{n}(k) \cdot \boldsymbol{\sigma} = n_x(k)\sigma_x + n_y(k)\sigma_y$ with $n_x = t + \cos k$ and $n_y = \sin k$. When $\mu = 0$, the term of σ_z vanishes and the model reduces to the chiral non-Hermitian SSH model which fulfills the chiral symmetry [16]:

$$\sigma_z \mathcal{H}(k) \sigma_z = -\mathcal{H}(k).$$

The chiral symmetry is broken when $\mu \neq 0$.

From Eq.(7), it is straightforward to get the square of eigenvalues given by

$$E^2(k) = t^2 + 1 + 2t \cos k - \delta^2 - \mu^2 - 2i\delta \sin k,$$

which suggests the existence of two solutions E_1 and E_2 with $E_2 = -E_1$. The i -th band energy $E_{1,2}$ can be represented as $E_i(k) = |E_i(k)|e^{i\theta_i(k)}$ ($i = 1, 2$) where $\theta_2(k) = \theta_1(k) + \pi = \theta(k) + \pi$. Substituting $E_{1,2}$ into Eq.(2), we can simplify ν_E to

$$\nu_E = \frac{1}{4} \sum_i \text{sgn}(\delta) \text{sgn}\left(\frac{\partial n_y}{\partial k} \Big|_{K_i}\right) \cdot \text{sgn}\left((n_x^2 - \delta^2 - \mu^2) \Big|_{K_i}\right), \quad (8)$$

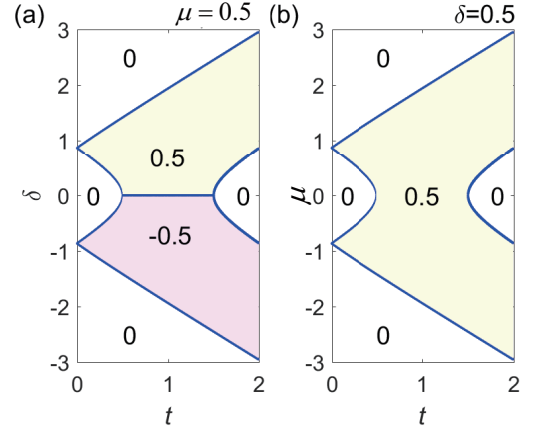


FIG. 1. Phase diagram characterized by the winding number of energy ν_E . (a) t versus δ by fixing $\mu = 0.5$, and (b) t versus μ by fixing $\delta = 0.5$. The light yellow shallow represents the winding number of energy $\nu_E = 0.5$ and the light pink shallow represents $\nu_E = -0.5$, while other regimes are $\nu_E = 0$. The phase transition is accompanied by the band touching (close of band gap).

where $k = K_i$ is the i -th solution of $n_y = 0$, which gives $k = 0$ and π . In Fig.1 we show the phase diagram of the model (5) with different phases characterized by different ν_E . In Fig.1(a), the phase diagram is plotted for t versus δ by fixing $\mu = 0.5$, and Fig.1(b) is for t versus μ by fixing $\delta = 0.5$. We find that the phase boundaries can be determined by $\delta^2 + \mu^2 = (t \pm 1)^2$, which is consistent with the band-touching (gap-closing) condition $E_1(k) = E_2(k) = 0$, i.e., the two bands touch together at the phase boundaries.

It is shown that in some regions of the phase diagram ν_E takes the half integer $\pm 1/2$, which suggests the definition Eq.(2) is not a true winding number in the geometrical meaning. The reason behind this is that in this region the complex eigenvalue $E_1(k)$ or $E_2(k)$ does not form a close curve when k goes around the BZ. To see it clear, we show $E_i(k)$ versus k in Fig.2, in which $E_i(k)$ changes continuously and smoothly with k . As shown in Fig.2 (b), neither E_1 nor E_2 form a close curve as k changes from $-\pi$ to π , instead they switch each other with $E_1(\pi) = E_2(-\pi)$ and $E_2(\pi) = E_1(-\pi)$, in contrast with the phase regimes with $\nu_E = 0$ corresponding to Fig.2 (a) and (c), where both $E_{1,2}(k)$ forms a close curve and we have $E_i(\pi) = E_i(-\pi)$.

Furthermore, we demonstrate that the definition Eq.(2) is equivalent to half of the difference of two winding numbers, i.e.,

$$\nu_E = \frac{1}{2} \text{sgn}(\delta)(\nu_2 - \nu_1), \quad (9)$$

where $\nu_{1,2} = \frac{1}{2\pi} \oint dk \nabla_k \phi_{1,2}$ with $\phi_{1,2}$ defined by

$$\tan \phi_1 = \frac{n_y}{n_x + \sqrt{\mu^2 + \delta^2}}, \quad \tan \phi_2 = \frac{n_y}{n_x - \sqrt{\mu^2 + \delta^2}}.$$

It is clear that ν_1 and ν_2 represent the winding number of the closed curve formed by $(n_x(k), n_y(k))$ in the two-dimensional

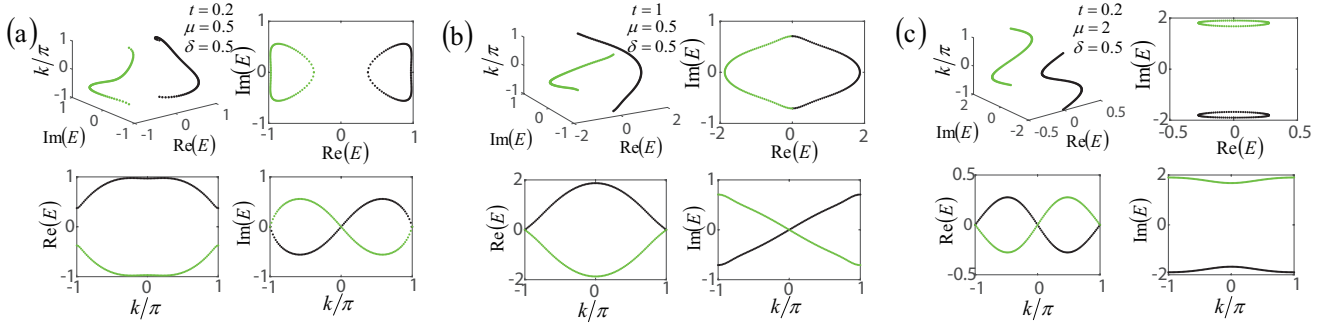


FIG. 2. Energy distribution in different parameter regions. The green curve and the black one represent E_1 and E_2 , respectively. The detailed parameters are shown in the figure. (a) and (c) correspond to $\nu_E = 0$, and (b) corresponds to $\nu_E = 0.5$.

space surrounding the EPs $(-\sqrt{\mu^2 + \delta^2}, 0)$ and $(\sqrt{\mu^2 + \delta^2}, 0)$, respectively.

IV. TOPOLOGICAL PROPERTIES OF EIGENVECTORS

A. Topological invariant of eigenvectors

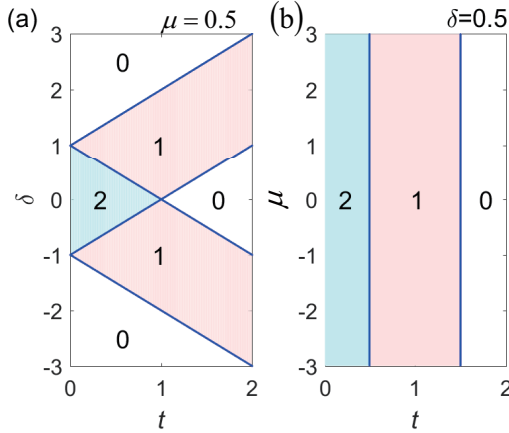


FIG. 3. Phase diagram characterized by topological invariant ν_{tot} . (a) t versus δ by fixing $\mu = 0.5$ and (b) t versus μ by fixing $\delta = 0.5$. The number in different color areas represents the topological invariant $\nu_{tot} = \nu_{s,1} + \nu_{s,2}$.

By using the expression of Eq.(4) and substituting it into $\nu_{tot} = \nu_{s,1} + \nu_{s,2}$, we get

$$\nu_{tot} = \frac{1}{2\pi} \oint dk \left[\frac{h_x \partial_k h_y - h_y \partial_k h_x}{E_1(E_1 - h_z)} + \frac{h_x \partial_k h_y - h_y \partial_k h_x}{E_2(E_2 - h_z)} \right].$$

With the help of the relation $E_2 = -E_1$, the above equation can be rewritten as

$$\begin{aligned} \nu_{tot} &= \frac{1}{2\pi} \oint dk \left[\frac{h_x \partial_k h_y - h_y \partial_k h_x}{E_1(E_1 - h_z)} + \frac{h_x \partial_k h_y - h_y \partial_k h_x}{E_1(E_1 + h_z)} \right], \\ &= \frac{1}{\pi} \oint dk \frac{h_x \partial_k h_y - h_y \partial_k h_x}{E_1^2 - h_z^2}. \end{aligned}$$

Since $E_1^2 = h_x^2 + h_y^2 + h_z^2$, we can get

$$\nu_{tot} = \frac{1}{\pi} \oint dk \frac{h_x \partial_k h_y - h_y \partial_k h_x}{h_x^2 + h_y^2}, \quad (10)$$

where $h_x = n_x = t + \cos k$ and $h_y = n_y + i\gamma_y = \sin k + i\delta$. We notice that ν_{tot} is independent of h_z , although its definition is related to the eigenvectors of $\mathcal{H}(k)$.

In Fig.3, we show the phase diagram characterized by different values of ν_{tot} . In Fig.3(a), the phase diagram is plotted for t versus δ by fixing a $\mu = 0.5$, and Fig.3(b) is for t versus μ by fixing a $\delta = 0.5$. Fig.3(b) clearly indicates that the phase diagram is irrelevant to μ as the expression of ν_{tot} is independent of h_z . From the expression of Eq.(10), we can see that the phase diagram shown in Fig.3(a) is identical to the phase diagram of the Hamiltonian in the absence of h_z term, i.e., the non-Hermitian Hamiltonian with chiral symmetry given by

$$\mathcal{H}_{chiral}(k) = (t + \cos k)\sigma_x + (\sin k + i\delta)\sigma_y. \quad (11)$$

The expression Eq.(10) does not represent a winding number in the geometrical meaning as $h_y(k)$ is not a real function. Following the same derivation for the case with chiral symmetry [16], we can represent ν_{tot} as the summation of two true winding numbers

$$\nu_{tot} = \nu'_1 + \nu'_2, \quad (12)$$

where $\nu'_{1,2} = \frac{1}{2\pi} \oint dk \nabla_k \phi'_{1,2}$ with $\phi'_{1,2}$ defined by

$$\tan \phi'_1 = \frac{n_y}{n_x + \delta}, \quad \tan \phi'_2 = \frac{n_y}{n_x - \delta}.$$

It is clear that ν'_1 and ν'_2 represent the winding number of the closed curve formed by $(n_x(k), n_y(k))$ in the two-dimensional space surrounding two points $(-\delta, 0)$ and $(\delta, 0)$, respectively. These two points are not EPs of the Hamiltonian (7), instead they are EPs of $\mathcal{H}_{chiral}(k)$. Consequently, the phase boundary of the phase diagram determined by ν_{tot} is same with the band touching condition for the system described by $\mathcal{H}_{chiral}(k)$, but is different from the phase diagram determined by ν_E .

Alternatively, we can also understand the geometrical meaning of the topological invariant ν_{tot} from trajectories of

eigenvectors by projecting the eigenvectors onto a 2D unit spherical surface. In general, the right-eigenvector can be parameterized as

$$|\psi_R(\alpha_k, \beta_k)\rangle = \begin{pmatrix} \cos \frac{\beta_k}{2} \\ e^{i\alpha_k} \sin \frac{\beta_k}{2} \end{pmatrix}, \quad (13)$$

For each eigenvector corresponding to E_1 or E_2 , we may calculate the sphere vector defined as $\mathbf{R}(k) = (\cos \alpha_k \sin \beta_k, \sin \alpha_k \sin \beta_k, \cos \beta_k)$, where α_k and β_k correspond to the azimuthal and polar angles of $\mathbf{R}(k)$, respectively. In Fig.4, we plot the evolution of two eigenvectors on the Bloch sphere across the Brillouin zone. Their trajectories form separately two closed curves as shown in Fig.4 (a) and (c), or form together a close curve in Fig.4 (b). The topological invariant ν_{tot} can be viewed as a winding number which accounts times of the trajectories passing around the z-axis connecting north and south poles.

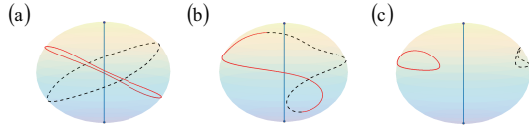


FIG. 4. The unit sphere vector $\mathbf{R}(k)$ (red curve with eigenvalue E_1 and black one with eigenvalue E_2). The parameter t in (a), (b) and (c) takes 0, 1 and 2, respectively, with other parameters $\mu = 0.5$ and $\delta = 0.5$. The blue line connects the north and south poles.

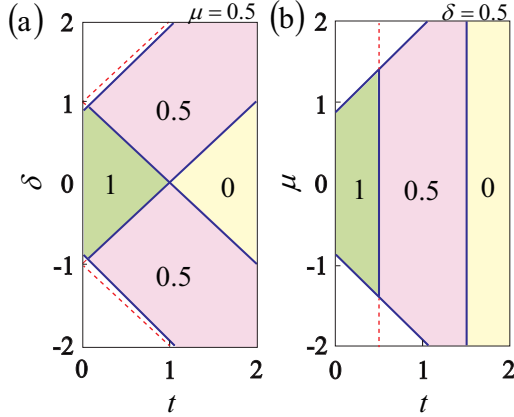


FIG. 5. Phase diagram characterized by the real part of Berry phase $\nu_{s,1}$. (a) t versus δ by fixing $\mu = 0.5$, and (b) t versus μ by fixing $\delta = 0.5$. The number in different color areas represents the quantized $\text{Re}(\nu_{s,1})$, and in the regions without the number $\text{Re}(\nu_{s,1})$ is not quantized. The blue solid curve represents the phase boundary of phase diagram characterized by $\text{Re}(\nu_{s,1})$, and the red dashed is corresponding to the phase boundary of ν_{tot} .

Generally speaking, $\nu_{s,1}$ is not quantized for a system without the chiral symmetry. However, for the model described by Eq.(7), the Hamiltonian satisfies a pseudo-inversion symmetry:

$$\sigma_x \mathcal{H}(k) \sigma_x = \mathcal{H}^\dagger(-k), \quad (14)$$

and we find that the real part of $\nu_{s,1}$ is quantized in some parameter regions due to the existence of the pseudo-inversion symmetry. Given that $\mathcal{H}(k)|\psi_\alpha^R(k)\rangle = E_\alpha(k)|\psi_\alpha^R(k)\rangle$, it follows

$$\mathcal{H}^\dagger(-k)\sigma_x|\psi_\alpha^R(k)\rangle = E_\alpha(k)\sigma_x|\psi_\alpha^R(k)\rangle.$$

Noticing that $\mathcal{H}^\dagger(-k)|\psi_\alpha^L(-k)\rangle = E_\alpha^*(-k)|\psi_\alpha^L(-k)\rangle$, we have $E_1(k) = E_1^*(-k)$ if the state fulfills $\sigma_x|\psi_1^R(k)\rangle = |\psi_1^L(-k)\rangle$ or $E_1(k) = E_2^*(-k)$ if the state fulfills $\sigma_x|\psi_1^R(k)\rangle = |\psi_2^L(-k)\rangle$. The difference between these two cases can be distinguished by whether the real part of $\nu_{s,1}$ is quantized or not. The real part of $\nu_{s,1}$ is quantized in the case of $E_1(k) = E_1^*(-k)$, and $\nu_{s,1}$ is not quantized but real in the other case. In Fig.5, regions labeled by quantized number 0, 0.5, 1 correspond to the case of $E_1(k) = E_1^*(-k)$ with quantized real part of $\nu_{s,1}$. Regions without labeled numbers correspond to the case of $E_1(k) = E_2^*(-k)$, for which $\nu_{s,1}$ is no longer quantized. The boundaries between these two cases can be determined by $E_{1,2}^2(k=0) = 0$ (see appendix B for details).

When the chemical potential term h_z is no longer imaginary, i.e., $h_z \equiv n_z + iy_z = \eta + i\mu$ with nonzero η , the pseudo-inversion system is broken, and the real part of $\nu_{s,1/2}$ is not quantized. Nevertheless, ν_{tot} is always quantized and takes the same value no matter which form h_z takes, i.e., the expression of Eq.(12) is irrelevant to the term of h_z .

B. Detection of phase boundaries via fidelity approach

We have demonstrated that the phase diagram determined by ν_{tot} displays quite different phase boundaries from the band-touching conditions. As ν_{tot} reflects the global geometrical properties of wavefunctions, we apply the fidelity approach to detect the phase boundaries. The fidelity approach has been widely used to study the phase transitions in various quantum many-body systems [59–63]. Given a Hamiltonian $H(\lambda)$, which depends on the driving parameter λ , the quantum fidelity is defined as the overlap between two eigenstates with only slightly different values of the external parameter and thus is a pure geometrical quantity. For the non-Hermitian Hamiltonian studied in this work, the driving parameter λ can be taken as t , δ or μ . In terms of the eigenstates $|\psi_{R,n}(\lambda)\rangle$ of $H(\lambda)$, the Hamiltonian can be reformulated as $H(\lambda) = \sum_n E_n(\lambda)|\psi_{R,n}(\lambda)\rangle\langle\psi_{L,n}(\lambda)|$. Therefore, we can generalize the definition of the state fidelity to the non-Hermitian system, which is defined as the half sum of the overlap between $|\psi_{R,1}(\lambda + \epsilon)\rangle$ and $|\psi_{L,1}(\lambda)\rangle$ and the overlap between $|\psi_{L,1}(\lambda + \epsilon)\rangle$ and $|\psi_{R,1}(\lambda)\rangle$, i.e.,

$$F(\lambda, \epsilon) = \frac{1}{2} |\langle\psi_{L,1}(\lambda)|\psi_{R,1}(\lambda + \epsilon)\rangle + \langle\psi_{R,1}(\lambda)|\psi_{L,1}(\lambda + \epsilon)\rangle|, \quad (15)$$

where $|\psi_{R,1}(\lambda)\rangle$ is the wavefunction corresponding to the parameter λ with eigenenergy E_1 and ϵ is a small quantity. It is obvious that the fidelity is dependent of ϵ . The rate of change of fidelity is given by the second derivative of fidelity or fidelity susceptibility

$$S(\lambda) = \lim_{\epsilon \rightarrow 0} \partial_\epsilon^2 \ln F(\lambda, \epsilon), \quad (16)$$

which is independent of ϵ . We note that the first derivative of fidelity defined by Eq.(15) gives zero, which is consistent with the Hermitian system [60–62].

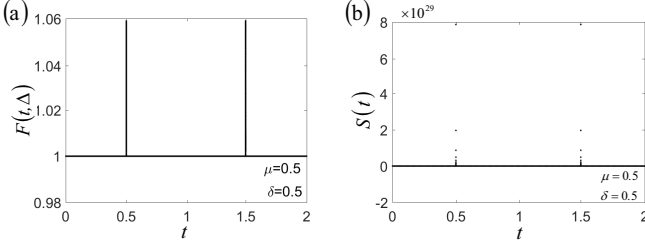


FIG. 6. The fidelity (a) and fidelity susceptibility (b) as a function of t . Here we take $\lambda = t$, $\mu = 0.5$ and $\delta = 0.5$.

In Fig.6, we display the fidelity and fidelity susceptibility versus the driving parameter t , i.e., we take $\lambda = t$, by fixing $\delta = 0.5$ and $\mu = 0.5$. It is shown that both the fidelity and fidelity susceptibility exhibit an abrupt jump in the vicinity of the transition points, which are consistent with the phase boundaries of the phase diagram determined by ν_{tot} . If we take the driving parameter as δ by fixing t and μ , similarly we find an abrupt jump of the fidelity and fidelity susceptibility in the vicinity of the transition points. Our results demonstrate that the phase transition point determined by the fidelity approach is different from that obtained by using Landau's energy criterion, which gives the phase boundaries by the band crossing condition. For the Hermitian system, it has been demonstrated that the fidelity susceptibility and the second derivatives of ground energy play an equivalent role in identifying the quantum phase transition. However, for the non-Hermitian system, they play different roles and may give different phase boundaries when the chiral symmetry is broken. This also explains why the discrepancy of phase diagrams determined by ν_E and ν_{tot} may arise for the non-Hermitian system.

V. SUMMARY

In summary, we have studied 1D general non-Hermitian systems without chiral symmetry and found the existence of discrepancy between phase diagrams characterized by two independent topological invariants ν_E and ν_{tot} , which are quantized for our studied systems. While the phase boundaries between phases with different ν_E are determined by the band-touching condition, the phase boundaries between different ν_{tot} are irrelevant to the band touching of the non-chiral system. The discrepancy of phase diagrams can be further clarified from the geometrical meaning the topological invariants ν_E and ν_{tot} , which can be represented as $\nu_E = \pm(\nu_2 - \nu_1)/2$ and $\nu_{tot} = \nu'_2 + \nu'_1$, where ν_1 and ν_2 are winding numbers counting the times of trajectory of the Hermitian part of the Hamiltonian encircling two EPs of the non-chiral Hamiltonian, and ν'_1 and ν'_2 are winding numbers associated with two EPs of the Hamiltonian in the absence of the chiral-symmetry breaking term. The fact that the topological invariant ν_{tot} is independent of the chiral-symmetry breaking term suggests that the corre-

sponding transition between different ν_{tot} is irrelevant to the band-touching points, instead it is equal to the winding number which counts times of trajectories of vectors by projecting the eigenstates onto 2D unit sphere passing around the z-axis connecting north and south poles. Furthermore, we find the existence of a hidden pseudo-inversion symmetry and the real part of $\nu_{s,\alpha}$ is quantized when the eigenvalues of the system satisfy $E_{1,2}(k) = E_{1,2}^*(-k)$.

We then generalize the definition of fidelity and use the fidelity and fidelity susceptibility to identify the phase transition in the non-Hermitian system. Our results show that an abrupt change of fidelity and fidelity susceptibility occurs around transition points between phases with different ν_{tot} , which suggests that the fidelity approach can witness topological phase transitions characterized by ν_{tot} accompanied with no gap closing in the non-Hermitian system. Our work unveils that the non-Hermitian systems may exhibit some peculiar properties, which have no correspondence in the Hermitian systems and are worthy of further investigation. A question that remains open is to find physical observable quantities to detect the topological invariants in the non-Hermitian models without chiral symmetry.

ACKNOWLEDGMENTS

The work is supported by NSFC under Grants No. 11425419, the National Key Research and Development Program of China (2016YFA0300600 and 2016YFA0302104) and the Strategic Priority Research Program (B) of the Chinese Academy of Sciences (No. XDB07020000).

Appendix A: The winding of eigenenergy ν_E

The winding number of energies ν_E can be written as

$$\nu_E = \frac{1}{2\pi} \int \nabla_{\mathbf{k}} \text{Arg}(\Delta E) d\mathbf{k},$$

where ΔE represents the difference of energies between any of the two bands. Generally speaking, a 2-band non-Hermitian system can be described by the Hamiltonian in Eq.(1), with eigenvalues $E_{1,2}^2 = |\mathbf{h}(k)|^2$ ($E_1 = -E_2$). Hence the angle of ΔE is half of the angle of $E_{1,2}^2$, and as a result ν_E can be interpreted as the half of the winding number of $E_{1,2}^2$ in the complex plane around the origin. In Hermitian systems, the energy $E_{1,2}$ is real and ν_E is always zero.

Similar to Ref.[64], the winding number of ν_E can be written as

$$\nu_E = \frac{1}{4} \sum_i \left(\text{sgn} \left(\frac{\partial \text{Im}(E_{1,2}^2)}{\partial \mathbf{k}} \right) \Big|_{\mathbf{k}=\mathbf{K}_i} \cdot \text{sgn}(\text{Re}(E_{1,2}^2)(\mathbf{K}_i)) \right), \quad (\text{A1})$$

with \mathbf{K}_i being the i -th solution of $\text{Im}(E_{1,2}^2) = 0$. For the Hamiltonian described by Eq.(7), the eigenvalues satisfy $E_{1,2}^2 = t^2 + 1 + 2t \cos k - \delta^2 - \mu^2 + 2i\delta \sin k$. It's easy to get

simplified form of v_E ,

$$v_E = \frac{1}{4} \sum_i \text{sgn}(\delta) \text{sgn}\left(\frac{\sin k}{\partial \mathbf{k}} |_{\mathbf{K}_i}\right) \text{sgn}((t^2 + 1 + 2t \cos k - \delta^2 - \mu^2) |_{\mathbf{K}_i}). \quad (\text{A2})$$

with \mathbf{K}_i is the i -th solution of $\sin k = 0$. This is different from the Hermitian cases where \mathbf{K}_i is determined by $\hat{h}_0 = 0$.

Now we give the geometric meaning of the winding number v_E . To see this, we parameterize the square of energies by:

$$E_{1,2}^2 = |E|^2 e^{2i\theta_k},$$

with

$$\tan 2\theta_k = \frac{2\delta \sin k}{t^2 + 1 + 2t \cos k - \delta^2 - \mu^2} = \frac{\text{Im}(E_{1,2}^2)}{\text{Re}(E_{1,2}^2)}.$$

then the winding number can be written as

$$\begin{aligned} 2\pi v_E &= \oint dk \nabla_k \theta_k = \oint dk \frac{1}{2} \cos 2\theta \nabla_k \tan 2\theta \\ &= \frac{2\text{Re}(E_{1,2}^2)}{|E_{1,2}^2|^2} \nabla_k \frac{\text{Im}(E_{1,2}^2)}{\text{Re}(E_{1,2}^2)} \\ &= \oint dk \frac{\text{Re}(E_{1,2}^2) \nabla_k \text{Im}(E_{1,2}^2) - \text{Im}(E_{1,2}^2) \nabla_k \text{Re}(E_{1,2}^2)}{2|E_{1,2}^2|^2} \\ &= \oint dk \frac{\text{Re}(E_{1,2}^2) \nabla_k \alpha \text{Im}(E_{1,2}^2) - \alpha \text{Im}(E_{1,2}^2) \nabla_k \text{Re}(E_{1,2}^2)}{2(\text{Re}(E_{1,2}^2)^2 + \alpha^2 \text{Im}(E_{1,2}^2)^2)} \\ &= \text{sgn}(\alpha) \oint dk \nabla_k \theta', \end{aligned}$$

where $\tan 2\theta' = \frac{\alpha \text{Im}(E_{1,2}^2)}{\text{Re}(E_{1,2}^2)}$. Here α is independent of k and taken to be $\alpha = \frac{\sqrt{\mu^2 + \delta^2}}{\delta}$, thus $\text{sgn}(\alpha) = \text{sgn}(\delta)$. The winding number of θ_k is now represented by the winding number of θ'_k as shown in Fig. 7(a). Furthermore, we have

$$\begin{aligned} \text{Re}(E_{1,2}^2) + i\alpha \text{Im}(E_{1,2}^2) &= \sqrt{(\text{Re}(E_{1,2}^2)^2 + \alpha^2 \text{Im}(E_{1,2}^2)^2)} e^{2i\theta'} \\ &= \sqrt{(\text{Re}(E_{1,2}^2)^2 + \alpha^2 \text{Im}(E_{1,2}^2)^2)} e^{-i\phi_1} e^{i\phi_2}, \end{aligned}$$

with $\tan \phi_1 = \frac{n_y}{n_x + \sqrt{\mu^2 + \delta^2}}$ and $\tan \phi_2 = \frac{n_y}{n_x - \sqrt{\mu^2 + \delta^2}}$, where $n_x = t + \cos k$ and $n_y = \sin k$. Here ϕ_1 and ϕ_2 are the angles of vector $\mathbf{n}(k)$ around the two EP points EP_1 and EP_2 as shown in Fig. 7(b), respectively. Finally, the winding number v_E becomes

$$v_E = \text{sgn}(\delta) \frac{1}{2\pi} \oint dk \nabla_k \theta' = \frac{1}{2} \text{sgn}(\delta) (v_2 - v_1), \quad (\text{A3})$$

where $v_i = \frac{1}{2\pi} \oint dk \nabla_k \phi_i$. Hence v_E measures the differences of winding number v_1 and v_2 , which is similar to the case of chiral Hamiltonian discussed in Ref.[16].

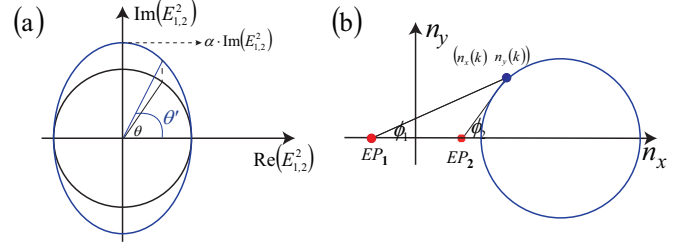


FIG. 7. (a) A schematic diagram of compressive deformation $E_{1,2}^2$. (b) A schematic diagram shows the geometrical meaning of ϕ_1 and ϕ_2 with $n_{x/y} = \text{Re} \langle \sigma_{x/y} \rangle$

Appendix B: The winding of eigenstate v_s

The eigenstates for non-Hermitian Hamiltonian satisfy

$$\begin{aligned} H(\mathbf{k}) |\psi_{1,2}^R\rangle &= E_{1,2} |\psi_{1,2}^R\rangle, \\ \langle \psi_{1,2}^L | H^\dagger(\mathbf{k}) &= \langle \psi_{1,2}^L | E_{1,2}, \end{aligned}$$

with

$$\begin{aligned} |\psi_{1,2}^R\rangle &= \frac{1}{\sqrt{2E_{1,2}(E_{1,2} - h_z)}} \begin{pmatrix} h_x - ih_y, E_{1,2} - h_z \end{pmatrix}^T, \\ \langle \psi_{1,2}^L | &= \frac{1}{\sqrt{2E_{1,2}(E_{1,2} - h_z)}} \begin{pmatrix} h_x + ih_y, E_{1,2} - h_z \end{pmatrix}, \end{aligned}$$

where the superscript T is transpose operation. The Berry phase v_s of the state is defined by

$$v_{s,1} = \frac{1}{\pi} \oint dk \langle \psi_1^L | i \partial_k | \psi_1^R \rangle.$$

Substituting the expression of $|\psi_1^R\rangle, \langle \psi_1^L|$ into this equation, v_s is rewritten as

$$\begin{aligned} v_{s,1} &= \frac{1}{\pi} \oint dk \frac{1}{\sqrt{2E_1(E_1 - h_z)}} \begin{pmatrix} h_x + ih_y & E_1 - h_z \end{pmatrix} \\ &\quad i \partial_k \frac{1}{\sqrt{2E_1(E_1 - h_z)}} \begin{pmatrix} h_x - ih_y \\ E_1 - h_z \end{pmatrix} \\ &= \frac{1}{\pi} \oint dk \frac{h_x \partial_k h_y - h_y \partial_k h_x}{2E_1(E_1 - h_z)}, \end{aligned}$$

Summing up the Berry phases of the two bands, the total Berry phase is

$$v_{\text{tot}} = v_{s,1} + v_{s,2} = \frac{1}{\pi} \oint dk \frac{h_x \partial_k h_y - h_y \partial_k h_x}{h_x^2 + h_y^2},$$

which can be proved to be quantized.

In a Hermitian system, a Hamiltonian having inversion symmetry means there is an unitary operator satisfying $UH(k)U^{-1} = H(-k)$. As a comparison, we can define a pseudo-inversion symmetry in the non-Hermitian system. Because of $H(k) \neq H^\dagger(k)$, the pseudo-inversion symmetry now requires $UH(k)U^{-1} = H^\dagger(-k)$, while the operator U is still

unitary. For example, if U is chosen to be σ_x , the pseudo-inversion symmetry gives some constraints on the Hamiltonian, i.e.,

$$\begin{aligned} h_x(k) &= h_x^*(-k), \\ h_y(k) &= -h_y^*(-k), \\ h_z(k) &= -h_z^*(-k). \end{aligned}$$

Besides, the eigenvalues should satisfy $E_1(k) = E_1^*(-k)$, or $E_1(k) = E_2^*(-k)$. Now we study the Berry phase for these two cases, respectively.

In the first case, we have $E_1(k) = E_1^*(-k)$, and the Berry phase $\nu_{s,1}$ is

$$\begin{aligned} \nu_{s,1} &= \frac{1}{\pi} \int_{-\pi}^{\pi} dk \langle \psi_1^L | i \partial_k | \psi_1^R \rangle \\ &= \frac{1}{\pi} \int_{-\pi}^{\pi} dk dk \frac{h_x(k) \partial_k h_y(k) - h_y(k) \partial_k h_x(k)}{2E_1(k)(E_1(k) - h_z(k))} \\ &= \frac{1}{\pi} \int_{-\pi}^{\pi} dk \frac{-h_x^*(-k) \partial_k h_y^*(-k) + h_y^*(-k) \partial_k h_x^*(-k)}{2E_1^*(-k)(E_1^*(-k) + h_z^*(-k))} \\ &= \frac{1}{\pi} \int_{-\pi}^{\pi} d(-k) \frac{h_x^*(-k) \partial_{-k} h_y^*(-k) - h_y^*(-k) \partial_{-k} h_x^*(-k)}{2E_1^*(-k)(E_1^*(-k) + h_z^*(-k))} \quad (k \rightarrow -k) \\ &= \frac{1}{\pi} \int_{-\pi}^{\pi} dk \frac{h_x^*(k) \partial_k h_y^*(k) - h_y^*(k) \partial_k h_x^*(k)}{2E_2^*(k)(E_2^*(k) - h_z^*(k))} \\ &= \frac{1}{\pi} \int_{-\pi}^{\pi} dk \langle \psi_2^R | i \partial_k | \psi_2^L \rangle \\ &= \nu_{s,2}^*. \end{aligned}$$

Similarity, we can see $\nu_{s,2} = \nu_{s,1}^*$. As a result, the total Berry

phase $\nu_{tot} = \nu_{s,1} + \nu_{s,2} = \nu_{s,1} + \nu_{s,1}^*$ is real and quantized. The real and imaginary part of $\nu_{s,1}$ satisfy $\text{Re}(\nu_{s,1}) = \text{Re}(\nu_{s,2}) = \frac{1}{2}\text{Re}(\nu_{tot})$; $\text{Im}(\nu_{s,1}) = \text{Im}(\nu_{s,2}^*)$. This phase is called pseudo-inversion symmetry unbroken phase, in which the real part of Berry phase $\nu_{s,i}$ is quantized.

In the second case, $E_1(k) = E_2^*(-k)$. The Berry phase $\nu_{s,1}$ is

$$\begin{aligned} \nu_{s,1} &= \frac{1}{\pi} \int_{-\pi}^{\pi} dk \langle \psi_1^L | i \partial_k | \psi_1^R \rangle \\ &= \frac{1}{\pi} \int_{-\pi}^{\pi} dk dk \frac{h_x(k) \partial_k h_y(k) - h_y(k) \partial_k h_x(k)}{2E_1(k)(E_1(k) - h_z(k))} \\ &= \frac{1}{\pi} \int_{-\pi}^{\pi} dk \frac{-h_x^*(-k) \partial_k h_y^*(-k) + h_y^*(-k) \partial_k h_x^*(-k)}{2E_2^*(-k)(E_2^*(-k) + h_z^*(-k))} \\ &= \frac{1}{\pi} \int_{-\pi}^{\pi} dk \frac{h_x^*(k) \partial_k h_y^*(k) - h_y^*(k) \partial_k h_x^*(k)}{2E_1^*(k)(E_1^*(k) - h_z^*(k))} \\ &= \frac{1}{\pi} \int_{-\pi}^{\pi} dk \langle \psi_1^R | i \partial_k | \psi_1^L \rangle \\ &= \nu_{s,1}^*. \end{aligned}$$

In this case, the $\nu_{s,1}$ and $\nu_{s,2}$ are real but not quantized. The phase is called pseudo-inversion symmetry broken phase.

-
- [1] C. M. Bender and S. Boettcher, Phys. Rev. Lett. **80**, 5243 (1998).
 - [2] C. M. Bender, Reports on Progress in Physics **70**, 947 (2007).
 - [3] Y. C. Hu and T. L. Hughes, Phys. Rev. B **84**, 153101 (2011).
 - [4] K. Esaki, M. Sato, K. Hasebe, and M. Kohmoto, Phys. Rev. B **84**, 205128 (2011).
 - [5] M. S. Rudner and L. S. Levitov, Phys. Rev. Lett. **102**, 065703 (2009).
 - [6] S.-D. Liang and G.-Y. Huang, Phys. Rev. A **87**, 012118 (2013).
 - [7] S. Longhi, Opt. Lett. **38** 3716 (2013); H. Schomerus, Opt. Lett. **38**, 1912 (2013).
 - [8] B. Zhu, R. Lü, and S. Chen, Phys. Rev. A **89**, 062102 (2014).
 - [9] S. Malzard, C. Poli, and H. Schomerus, Phys. Rev. Lett. **115**, 200402 (2015).
 - [10] T. E. Lee, Phys. Rev. Lett. **116**, 133903 (2016).
 - [11] D. Leykam, K. Y. Bliokh, C. Huang, Y. D. Chong, and F. Nori, Phys. Rev. Lett. **118**, 040401 (2017).
 - [12] Y. Xu, S.-T. Wang, and L.-M. Duan, Phys. Rev. Lett. **118**, 045701 (2017).
 - [13] J. Gonzales and R. A. Molina, Phys. Rev. B **96**, 045437 (2017).
 - [14] Y. Xiong, J. Phys. Commun. **2**, 035043 (2018).
 - [15] H. Shen, B. Zhen, and L. Fu, Phys. Rev. Lett. **120** 146402 (2018).
 - [16] C. Yin, H. Jiang, L. Li, R. Lü, and S. Chen, Phys. Rev. A **116**, 133903 (2018).
 - [17] J. M. Zeuner, M. C. Rechtsman, Y. Plotnik, Y. Lumer, S. Nolte, Mark S. Rudner, M. Segev, and A. Szameit, Phys. Rev. Lett. **115**, 040402 (2015).
 - [18] J. Gong and Q. Wang, Phys. Rev. A **82**, 012103 (2010).
 - [19] C. Yuce, Phys. Lett. A **379**, 1213 (2015).
 - [20] H. Shen and L. Fu, arXiv:1802.03023.
 - [21] S. Lieu, Phys. Rev. B **97**, 045106 (2018).
 - [22] Z. Gong, Y. Ashida, K. Kawabata, K. Takasan, S. Higashikawa and M. Ueda, Phys. Rev. X, **8**, 031079 (2018).
 - [23] S. Lieu, arXiv:1807.03320.
 - [24] K. Kawabata, S. Higashikawa, Z. Gong, Y. Ashida and M. Ueda, arXiv:1804.04676.
 - [25] C. Li, X. Z. Zhang, G. Zhang, and Z. Song, Phys. Rev. B **97**, 115436 (2018).
 - [26] K. L. Zhang, P. Wang, G. Zhang, and Z. Song, Phys. Rev. A **98**, 022128 (2018).
 - [27] Q. B. Zeng, S. Chen, and R. Lü Phys. Rev. A **95**, 062118 (2017); Q.-B. Zeng, B. Zhu, S. Chen, L. You, and R. Lü Phys. Rev. A **94**, 022119 (2016).
 - [28] L. Jin, Phys. Rev. A **96**, 032103 (2017).
 - [29] C. Yuce, Phys. Rev. A **98** 012111 (2018); Phys. Rev. A **97** 042118 (2018).
 - [30] T. E. Lee, F. Reiter, and N. Moiseyev, Phys. Rev. Lett. **113**, 250401 (2014).
 - [31] V. M. Martinez Alvarez, J. E. Barrios Vargas, L. E. F. Foa Torres

- Phys. Rev. B **97**, 121401(R) (2018).
- [32] V. M. Martinez Alvarez, J. E. Barrios Vargas, M. Berdakin, and L. E. F. Foa Torres, arXiv:1805.08200
 - [33] V. Kozii and L. Fu, arXiv:1708.05841.
 - [34] M. Papaj, H. Isobe and L. Fu, arXiv:1802.00443.
 - [35] J.-W. Ryu, S.-Y. Lee, and S. W. Kim, Phys. Rev. A **85**, 042101 (2012).
 - [36] Y. Ashida, S. Furukawa and M. Ueda, Nat. Commum. **8**, 15791 (2017).
 - [37] T. Chen, B. Wang, and X. D. Zhang Phys. Rev. A **97**, 052117 (2018).
 - [38] C. E. Ruter, K. G. Makris, R. El-Ganainy, D. N. Christodoulides, M. Segev, and D. Kip, Nat. Phys. **6**, 192 (2010).
 - [39] B. Peng, Sahin Kaya Özdemir, F. Lei, F. Monifi, M. Gianfreda, G. L. Long, S. Fan, F. Nori, C. M. Bender, and L. Yang, Nat. Phys. **10**, 394 (2014).
 - [40] L. Feng, Z. J. Wong, R.-M. Ma, Y. Wang, and X. Zhang, Science **346**, 972 (2014).
 - [41] V. V. Konotop, J. Yang, and D. A. Zezyulin, Rev. Mod. Phys. **88**, 035002 (2016).
 - [42] L. Xiao, X. Zhan, Z. H. Bian, K. K. Wang, X. Zhang, X. P. Wang, J. Li, K. Mochizuki, D. Kim, N. Kawakami, et al., Nat. Phys. **13**, 1117 (2017).
 - [43] S. Weimann, M. Kremer, Y. Plotnik, Y. Lumer, S. Nolte, K. G. Makris, M. Segev, M. C. Rechtsman, and A. Szameit, Nat. Mater. **16**, 433 (2017).
 - [44] H. Menke and M. M. Hirschmann, Phys. Rev. B **95**, 174506 (2017).
 - [45] M. Klett, H. Cartarius, D. Dast, J. Main and G. Wunner, arXiv:1802.06128.
 - [46] W. D. Heiss and H. L. Harney, Eur. Phys. J. D **17**, 149 (2001); W. D. Heiss, J. Phys. A Math. Theor. **45**, 444016 (2012).
 - [47] C. Dembowski, B. Dietz, H.-D. Gräf, H. L. Harney, A. Heine, W. D. Heiss, and A. Richter, Phys. Rev. E **69**, 056216(2004).
 - [48] M. V. Berry, Czech. J. Phys. **54**, 1039 (2004).
 - [49] I. Rotter, J. Phys. A Math. Theor. **42**, 153001 (2009).
 - [50] H. Jing, S. K. Özdemir, H. Lü, and F. Nori, Sci Rep **7** 3386 (2017).
 - [51] W. Hu, H. Wang, P. P. Shum and Y. D. Chong, Phys. Rev. B **95**, 184306 (2017).
 - [52] A. U. Hassan, B. Zhen, M. Soljačić, M. Khajavikhan, and D. N. Christodoulides, Phys. Rev. Lett. **118**, 093002 (2017).
 - [53] F. K. Kunst, E. Edvardsson, J. C. Budich, and E. J. Bergholtz, Phys. Rev. Lett. **121**, 026808 (2018).
 - [54] S. Yao and Z. Wang, Phys. Rev. Lett. **121**, 086803 (2018).
 - [55] S. Yao, F. Song and Z. Wang, Phys. Rev. Lett. **121**, 136802 (2018).
 - [56] C. Chiu, J. C. Y. Teo, A. P. Schnyder, and S. Ryu, Rev. Mod. Phys. **88**, 035005 (2016).
 - [57] J. Zak, Phys. Rev. Lett. **62**, 2747 (1989).
 - [58] L. Li, C. Yang, and S. Chen, EPL (Europhysics Letters) **112**, 10004 (2015).
 - [59] S. Zhu, Phys. Rev. Lett. **96**, 077206(2006).
 - [60] P. Zanardi and N Paunković, Phys. Rev. E **74**, 031123 (2006).
 - [61] W.-L. You, Y.-W. Li, and S.-J. Gu, Phys. Rev. E **76**, 022101 (2007).
 - [62] S. Chen, L. Wang, Y. Hao, and Y. Wang, Phys. Rev. A **77**, 032111 (2008).
 - [63] S. Chen, L. Wang, S.-J. Gu, and Y. Wang Phys. Rev. E **76**, 061108 (2007); Y. Ma, S. Chen, H. Fan, and W. Liu, Phys. Rev. B **81**, 245129 (2010).
 - [64] L. Zhang, L. Zhang, S. Niu, and X.-J. Liu, arXiv:1802.10061.